

# Non-Stationary Long-Term Dynamics via Selected Incomplete Dual Bases

Grace Hsiao-Han Chuang<sup>1\*</sup> and Abhijit Pendse<sup>1</sup>

<sup>1</sup>Max-Planck-Institute for the Physics of Complex System, Nöthnitzer Straße 38, Dresden, 01187, Germany.

\*Corresponding author(s). E-mail(s): [hhchuang@pks.mpg.de](mailto:hhchuang@pks.mpg.de);  
Contributing authors: [pendse@pks.mpg.de](mailto:pendse@pks.mpg.de);

## Abstract

Simulating the dynamics of non-stationary, long-term many-body quantum systems poses significant challenges due to the large size of the state space. We are examining how traditional basis sets struggle to accurately represent long-term dynamics when using incomplete sets. To address this issue, we propose using an SU(2) coherent state basis and deriving equations of motion for both time-independent and time-dependent Hamiltonian. This methodology involves a sampling approach, where a subset of relevant configurations is chosen based on energy criteria, and a projection method is used to enhance the accuracy of wavefunction propagation while reducing computational cost. We evaluate this method through numerical simulations of a seven-qubit system, calculating key physical observables such as state probabilities and domain-wall densities. Our results indicate that while complete basis sets offer accurate dynamics, selected incomplete sets can recover essential features, especially with the assistance of a projector. Our conclusion suggests that the selected incomplete dual basis method can efficiently capture both short-term and long-term dynamics.

## 1 Introduction

A chain of coupled two level atoms known as the Ising chain is the simplest form of a many body quantum system[1, 2]. An Ising chain with tunable parameters is of interest to study many body dynamics, phase transitions as well as for use in quantum technologies. An array of Rydberg atoms is one such realization of an Ising chain which has gained popularity in recent times [3, 2]. Rydberg atom chains have been

used to study many-body aspects of spin chains[4, 5] as well as its use in metrology[6] and quantum computation[7]. Rydberg atoms present a suitable platform due to the control on atom placement achieved using optical tweezers, as well as due to the long-range Rydberg-Rydberg interactions[8, 9].

While there has been considerable experimental progress in assembly of 1D and 2D arrays of Rydberg atoms[8, 10], numerical simulation of the dynamics of such large systems presents a challenge due to the large state space of the system. To simulate this system, one can numerically solve the time-dependent Schrödinger equation [11] by choosing a set of complete, orthonormal and time-independent basis functions  $\{|\zeta_i\rangle\}$  and writing the wavefunction as a linear combination of such a basis. The time-dependent part is described in the amplitudes [12, 13].

$$|\Psi(t)\rangle = \sum_{\ell}^N a_{\ell}(t)|\zeta_{\ell}\rangle, \quad (1)$$

where  $N$  is the size of the basis set  $\{|\zeta_i\rangle\}$ . Different type of basis functions are used in variety of problems, and Discrete Variable Representation (DVR) [14] is one of them to solve the time-dependent Schrödinger equation. The simplest method in DVR uses delta functions in space, while advanced DVR methods have also been proposed [15, 16]. As we need a complete set in this method, it suffers from exponential growth of the system size. In DVR method, it is broadly used but limited to few degrees of freedom [17, 18].

Unlike time-independent basis set functions, time-dependent basis set functions [19]  $\{|\xi_{\ell}(t)\rangle\}$  in general are not orthogonal ( $\langle\xi_{\ell}|\xi_m\rangle \neq 0$ ), but can be normalized ( $\langle\xi_{\ell}|\xi_m\rangle = 1$ ). The resulting wavefunction is also a linear combination of basis functions, and both amplitude and basis function are time-dependent.

$$|\Psi(t)\rangle = \sum_{\ell}^N a_{\ell}(t)|\xi_{\ell}(t)\rangle \quad (2)$$

In a recent work [20] coupled qubits have been realized experimentally as arrays of trapped Rydberg atoms. The many-body quantum state was controlled by the ratio of the distance between adjacent Rydberg atoms and the power of laser. Unexpected long-time dynamics have been observed, similar to long-term stable trajectories in classical systems [21]. State probabilities and the so-called domain wall densities are good observables, which can be used to compare calculated results with experiments.

The paper is organized as follows. In Section 2, the definition of the SU(2) coherent state (superposition of ground and Rydberg states) and the derivation of equations-of-motion are given, and follows two sampling schemes and a projection method. In Section 3, the numerical result of two physical observables, state probability and domain-wall density, are calculated to evaluate the effectiveness our method. We conclude by summarizing our results in section 4.

## 2 Methodology

### 2.1 Equation-of-Motion in the SU(2) Coherent State

We consider a chain of  $M$  atoms with their ground state given by  $|g\rangle$ , coupled to a Rydberg state  $|r\rangle$  using an external driving laser. The Rabi frequency for the Rydberg transition and the detuning are both spatially uniform, but time dependent. The general form of Hamiltonian for this system is

$$\frac{\hat{H}(t)}{\hbar} = \frac{\Omega(t)}{2} \sum_i^M \hat{\sigma}_x^i - \Delta(t) \sum_i^M \hat{n}_i + \sum_i^M \sum_{j \neq i}^M V_{ij} \hat{n}_i \hat{n}_j, \quad (3)$$

where  $\Omega(t)$  is the Rabi frequency,  $\Delta(t)$  is the laser detuning and  $V_{ij} \propto \frac{1}{R_{ij}^6}$  is the Van der Waals interaction between atoms at site  $i$  and  $j$ . In the Hamiltonian,  $\hat{\sigma}_x^i = |g_i\rangle \langle r_i| + |r_i\rangle \langle g_i|$  denotes the coupling between the ground state and Rydberg state for the  $i$ -th atom and  $\hat{n}_i = |r_i\rangle \langle r_i|$ .

We use coherent state as basis to expand the time-dependent state vector in equation (2). In a multidimensional case, this coherent state is a tensor product of spin coherent states of individual atoms,  $|\xi_\ell(t)\rangle = \bigotimes_i^M |\xi_\ell^i(t)\rangle$ . Each  $|\xi_\ell^i(t)\rangle$  is a  $SU(2)$  spin coherent state at the  $i^{\text{th}}$  site instead of a Gaussian coherent state. The total coherent state is then defined as

$$|\xi_\ell(t)\rangle = \bigotimes_i^M |\xi_\ell^i(t)\rangle = \bigotimes_i^M \frac{(\xi_\ell^i(t) + 1)|g_i\rangle + (\xi_\ell^i(t) - 1)|r_i\rangle}{\sqrt{2(1 + |\xi_\ell^i(t)|^2)}}, \quad (4)$$

where  $|g_i\rangle$  and  $|r_i\rangle$  are the two eigenstates of the  $i^{\text{th}}$  two level system or eigenvectors of the Pauli matrix,  $\sigma_z^i$ . We found the parametrisation as in Eq. (4) of spin coherent state more stable numerically than more common parametrization  $|\xi\rangle = \frac{|g\rangle + \xi|r\rangle}{\sqrt{1 + |\xi|^2}}$ .

In the common expression,  $|\xi\rangle \rightarrow |r\rangle$  as  $\xi \rightarrow \infty$  which has difficulty in numerical simulation. In equation (4),  $\xi_\ell^i$  is a complex number with magnitude in the range  $0 \leq |\xi| \leq 1$ , and  $\bar{\xi}_\ell^i$  is its complex conjugate. This coherent state basis,  $\{|\xi\rangle\}$ , are normalised ( $\langle \xi_\ell | \xi_\ell \rangle = 1$ ) to avoid nonphysical interpretation, but it is not orthogonal ( $\langle \xi_m | \xi_\ell \rangle \neq 0$  for  $m \neq \ell$ ). The corresponding overlap matrix is

$$\Omega_{ml} \equiv \langle \xi_m | \xi_\ell \rangle = \prod_i^M \frac{1 + \bar{\xi}_m^i \xi_\ell^i}{\sqrt{1 + |\xi_m^i|^2} \sqrt{1 + |\xi_\ell^i|^2}}. \quad (5)$$

To solve the time-dependent Schrödinger equation, we plug the wavefunction from equation (4) and the the Hamiltonian from equation (3) into it, and then the resulting

equation-of-motion in the time-dependent coherent state basis is

$$\dot{\vec{a}} = \boldsymbol{\Omega}^{-1}(-\mathbf{X} - i \mathbf{H}) \vec{a}, \quad (6)$$

$$\dot{\xi}_\ell^i = -i \left[ \Omega(t) \xi_\ell^i + \frac{(\xi_\ell^i)^2 - 1}{2} \left( -\Delta(t) + \sum_i^M \sum_{j \neq i}^M V_{ij} \frac{(\bar{\xi}_\ell^j - 1)(\xi_\ell^j - 1)}{1 + |\xi_\ell^j|^2} \right) \right]. \quad (7)$$

Equation (6) is the evolution for amplitude column vector, where matrix  $\mathbf{X}$  is a function of overlap matrix  $\boldsymbol{\Omega}$ , and their explicit form of matrix element of  $\mathbf{X}$  is in equation (A.3) and overlap  $\boldsymbol{\Omega}$  in equation (5).  $\mathbf{H}$  is the Hamiltonian matrix in coherent state basis and its matrix element is in equation (A.8). Equation (7) is the evolution of the total coherent state  $\ell$ , where the individual coherent state,  $|\xi_\ell^i\rangle$ , is derived by applying the variational principle. The complete derivation can be found in the Appendix A.

## 2.2 Sampling: construct incomplete basis

We choose spin coherent state as a basis for both time-dependent and independent basis function. Recall that from equation (1) and (2) of a time-dependent wavefunction, the time-dependent part is purely carried by amplitude in time-independent basis functions, and contributes to both amplitude and basis in time-dependent basis functions.

The size of complete basis set is  $2^M$  where  $M$  is the number of Rydberg atoms in a chain. Not all the basis functions are relevant in dynamics, and we want to select important basis functions to construct the total wavefunction. Equation (3) shows the connection of energy and configuration of Rydberg atom chain, and it indicates to use energy as a criteria to filter important configurations (basis functions). Because the third terms is the interaction between two Rydberg atoms at site  $i$  and  $j$  and it decreases rapidly ( $\frac{1}{R_{ij}^6}$ ) when the distance increase, the strongest interaction is the nearest neighbour interaction. As a result, we can build subset based on the configuration. We write down all the configurations, and select the one with no Rydberg atom or isolate Rydberg atoms as the first subset ( $C_{\text{iso}}$ ). We then add one pair of Rydberg atoms as the second subset ( $C_{\text{pair}}$ ). Finally, the complete basis set allows all the configurations ( $C_{\text{tot}}$ ). The analytical expression and detailed derivation of these subsets is shown in appendix B. In our simulation, we use three sets of basis function and their size is

$$C_{\text{tot}} > C_{\text{pair}} + C_{\text{iso}} > C_{\text{iso}} \quad (8)$$

A more general method to sample the subspace is Monte Carlo. The criteria of accepting states is the correlation between dominant state and satellite states, and their correlation is defined by the overlap matrix in equation 5. The process is illustrated as follows. First, a random number  $\xi'$  is generated in a normal distribution between  $-1$  and  $1$ , and this random number constructs satellite states.

### 3 Results

#### 3.1 Time-dependent Hamiltonian

In accordance with the experiment [20], to prepare the target state  $|\mathbb{Z}_2\rangle$  ( $|rgrgrgr\rangle$ ) from ground state  $|\mathbb{G}\rangle$  ( $|ggggggg\rangle$ ) by controlling the laser intensities, the time-dependent Hamiltonian described in equation (3) is given by:

$$\frac{\hat{H}(t)}{\hbar} = \frac{\Omega}{2} \sum_i^M \hat{\sigma}_x^i - \Delta(t) \sum_i^M \hat{n}_i + \sum_i^M \sum_{j=i\pm 1}^M V_{ij} \hat{n}_i \hat{n}_j. \quad (9)$$

Here, the Rabi oscillation ( $\Omega$ ) is a constant  $2\pi \times 2$  MHz within the time range of 0 to  $2.25 \mu\text{s}$ , and the time-dependent laser detuning ( $\Delta(t)$ ) is represented by the polynomial equation  $\Delta(t) = a + bt + ct^2 + dt^3$ , with coefficients  $a = -101.38$ ,  $b = 205.53$ ,  $c = -136.38$ , and  $d = 30.24$ , fitted from experimental data. We consider only the nearest neighbour repulsive van der Waals interaction between Rydberg atoms  $V_{i,i\pm 1} = 2\pi \times 24$  MHz in our model. The numerical wavefunction propagation is carried out using the Python library QuTip [22, 23].

For a seven-qubit system, its state probability calculated from the complete time-independent basis is shown in Figure (1). The complete basis is carried with classical configurations  $2^M$  where  $M = 7$ . The experiment [20] indicates that at the start, there

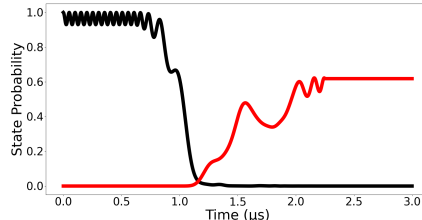


**Fig. 1:** State probabilities of a seven-qubit chain are calculated on a time-independent basis. Black: ground state, red:  $|\mathbb{Z}_2\rangle$  state.

is more than 80% ground state  $|\mathbb{G}\rangle$ . In the short-term dynamics ( $0-1 \mu\text{s}$ ) there is consistent oscillation followed by an immediate drop. We set the ground state probability at 100% at time  $t = 0$  and then replicate the aforementioned dynamics. Following this, the assessment of the long-term dynamics ( $1.5-3 \mu\text{s}$ ) is primarily influenced by the target state  $|\mathbb{Z}_2\rangle$ . The experiment shows that the  $|\mathbb{Z}_2\rangle$  probability ranges between 54% and 77%, while our simulation yields a probability of 61% for  $|\mathbb{Z}_2\rangle$ , validating this complete basis.

In order to determine the appropriate size of the subspace for calculating a state vector, we change various time-dependent bases. In Figure (2), we compute the probabilities of the states using different selected subspaces (refer to Section 2.2). To evaluate

the accuracy of the wavefunction, we compare the final target state  $|\mathbb{Z}_2\rangle$  in both a reduced and complete basis set.

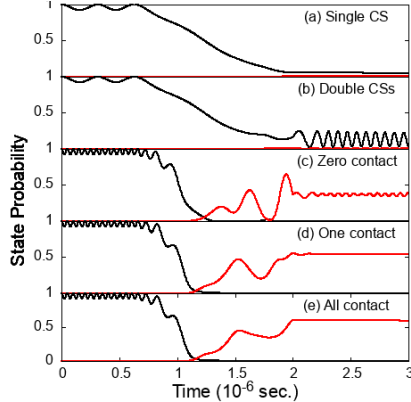


**Fig. 2:** State probabilities of a seven-qubit chain are calculated in several time-dependent coherent states. Black:  $|\mathbb{G}\rangle$  and red:  $|\mathbb{Z}_2\rangle$ . At  $t_0 = 0$ , the wavefunction is composed of (a) a single  $|\mathbb{G}\rangle$ , (b) both  $|\mathbb{G}\rangle$  and  $|\mathbb{Z}_2\rangle$ , (c) a subspace with an isolated configuration  $C_{\text{iso}}$  (34 bases), (d) a subspace with an isolated and pair configuration (72 bases), and (e) a complete basis (128 bases).

The quality of the chosen basis is evaluated by comparing the probability of the target state with the complete basis ( $|\mathbb{Z}_2|^2 = 60\%$  in Figure (2e)). In the two extreme cases shown in Figure (2a) and (2b), they both fail to capture both short-term and long-term dynamics. In case (a), only one coherent state with the  $|\mathbb{G}\rangle$  configuration is present, while in case (b), two coherent states are used (the  $|\mathbb{G}\rangle$  and  $|\mathbb{Z}_2\rangle$  configurations) at  $t_0$ . In the short term, the oscillation of the ground state probability is significantly slower than expected, and eventually reaches almost zero target state probability. Isolated and pair configuration is used in Figure (2c) and (2d). Case (c) composes only isolated configuration, and case (d) has both configurations. Both cases capture the short-term dynamics qualitatively - they oscillate consistently in the beginning and then drop down immediately. However, in case (c), the target state probability is only 39%, while in case (d), it is 53%.

A more generalized sampling scheme is used to calculate the probability of the state  $|\mathbb{Z}_2\rangle$ . The Monte Carlo method randomly selects states without prior information, and then compression parameters (CP) are used to increase the correlation between states. Three sizes of basis sets (34, 72, and 128) are chosen for a 7-qubit system to compare with the aforementioned configuration schemes. The compression parameter (CP) converges to  $CP = 15$  for both 34 and 72 bases, resulting in  $|\mathbb{Z}_2\rangle$  probabilities of 40% and 53%, respectively. For the complete set with 128 bases, no compression ( $CP = 1$ ) is applied, resulting in a 60%  $|\mathbb{Z}_2\rangle$  probability.

Even in the case of a coherent state, which is an overcomplete basis, increasing the CP too much causes overlap between two bases, leading to a singularity in the overlap matrix in equation (5).

Based on the quantitative evaluation, the smallest size of basis set is 72 bases for a 7-qubit system. In selected configurations, it is a  $C_{\text{iso}} + C_{\text{pair}}$  subspace. In Monte Carlo method, it needs  $CP = 15$  for the same size of basis.

### 3.2 Time-independent Hamiltonian

In the same experiment [20], the other physical observable, domain-wall density, is measured after turning off the laser detuning. It corresponds to a time-independent Hamiltonian

$$\frac{\hat{H}}{\hbar} = \frac{\Omega}{2} \sum_i^M \hat{\sigma}_x^i + \sum_i^M \sum_{j=i\pm 1}^M V_{ij} \hat{n}_i \hat{n}_j. \quad (10)$$

We initialize the system in the target state  $|\mathbb{Z}_2\rangle$  and propagate it with the above Hamiltonian, and then the system oscillates between two ordered states  $|\mathbb{Z}_2\rangle$  and  $|\mathbb{Z}'_2\rangle$  ( $|\text{rgrgrgr...}\rangle = |\text{grgrgrg...}\rangle$ ) in a short period. After that, states are randomized in the end. This oscillatory behaviour can be captured by measuring the domain-wall density, which is independent of the size of the qubit chain [20].

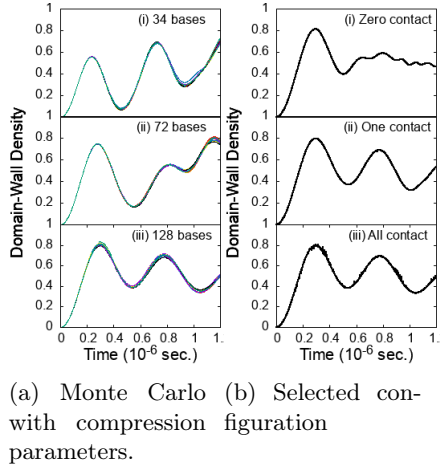


**Fig. 3:** Domain-wall density of a seven-qubit chain are calculated in two sampling schemes. (a) Monte Carlo with compression parameters and (b) selected configurations. The size of the basis are the same in the same row.

Two sampling schemes are used to construct a wavefunction (refer to Section 2.2 for details). In Figure 3a (i) and 3b (i), 34 bases are used in both sampling schemes, but they do not adequately describe the domain wall density either qualitatively or quantitatively. In Figure 3a (ii) and 3b (ii), 72 bases are used, and only the selected configuration ( $C_{\text{iso}} + C_{\text{pair}}$  subspace) captures the long-term oscillation after 0.5  $\mu\text{s}$ .

In Figure 3a (iii) and 3b (iii), with 128 bases, both schemes work for both short- and long-term oscillation. To describe the domain wall density, the best basis set is the  $C_{\text{iso}} + C_{\text{pair}}$  subspace with a size of 72.

### 3.3 Use of a projector to reduce basis size

From Figure (2) and (3), two physical observables (state probability and domain-wall density) corresponding to two Hamiltonians work well in the same  $C_{\text{iso}} + C_{\text{pair}}$  subspace. We push the limit to a smaller subspace of  $C_{\text{iso}}$  configurations only, and correct the non-stationary long-term dynamics by a projector and selected dual bases in Figure (4).

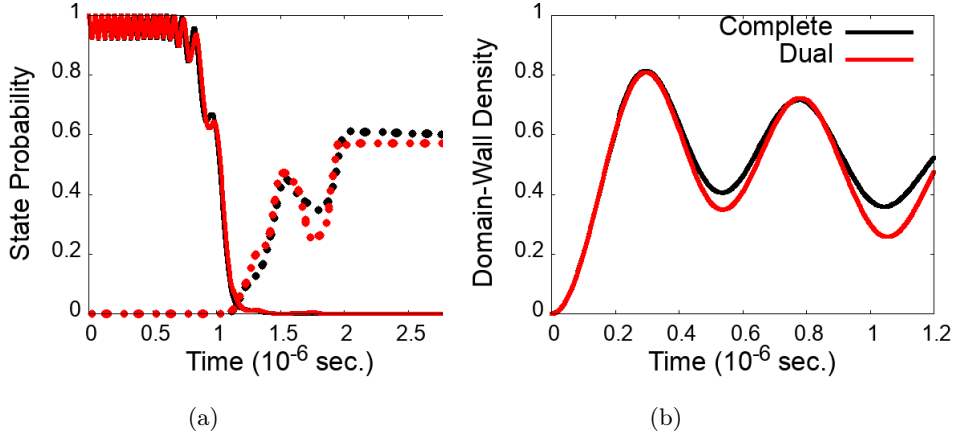


**Fig. 4:** Comparing the result of the complete basis set (128 bases) in the black line and dual bases (34 bases) in the red line with both (a) state probability and (b) domain-wall density. In (a), the solid line is  $|\mathbb{G}\rangle$  probability, and the dot line  $|\mathbb{Z}_2\rangle$  probability. In (b), black is complete basis, and red is dual bases.

In Figure (4a), we initialize our system in state  $|\mathbb{G}\rangle$ , and propagate it with equation (9).  $|\mathbb{Z}_2\rangle$  probability is 60% in the complete basis (black dot line in 4a), and 57% in the dual basis set (red dot line in 4a). With the same size (34 bases) of subspace, the  $|\mathbb{Z}_2\rangle$  probability is corrected from 39% to 57% after using the dual bases method in Figure (2c) and Figure (4a), respectively.

In Figure (4b), we initialize our system as  $|\mathbb{Z}_2\rangle$ , and propagate it with equation (10). The domain-wall density describes the oscillation between two states  $|\mathbb{Z}_2\rangle = |\mathbb{Z}'_2\rangle$  in a short period. Comparing with Figure 3b (i) which only captures the short-term dynamics (the first wave packet from 0 to  $0.5 \mu$ ) in  $C_{\text{iso}}$  subspace but fails to describe the non-stationary long-term dynamic. With the dual bases method, the long-term oscillation is restored with the same size of bases as shown in the red solid line in Figure (4b). After dual bases qualitatively restored the oscillation of domain-wall density, the quantitative comparison with complete basis is shown in the depth of

oscillation at 0.5 and 1.0  $\mu\text{s}$  in Figure (4b) that dual bases method has a deeper oscillation than complete basis.

## 4 Conclusion

In this article, we studied a seven-qubit chain for non-stationary long-term dynamics. We reduce the basis size by employing a projector in two selected bases without making any additional approximations. Using this reduced basis, we analyze the non-stationary long-term dynamics in both the probability of being in the state  $|\mathbb{Z}_2\rangle$  and the density of domain walls.

Both of the selected bases are SU(2) spin coherent states. One is an orthonormal and time-independent basis set, while the other is time-dependent and normalized. Since a coherent state is an overcomplete basis, there is a freedom to formulate multiple representations of a state vector. However, the drawback is the redundancy, which requires proper sampling schemes. Due to the fast decay of the interaction of Rydberg atoms as  $\frac{1}{R^6}$ , we use total energy to select the corresponding subspace.

After two subspaces are chosen, a state vector is rewritten using a projector. The  $|\mathbb{Z}_2\rangle$  probability increases from 39% to 57% (60% in the complete basis set), and the long-term oscillation of domain-wall density is restored as well. Future works can include next nearest neighbour interactions as required in some experiments [8].

**Acknowledgments.** We thank Dr. Francisco Gonzalez-Montoya, Dr. Jonathan Rawlinson, and Dr. Dmitry Shalashilin for the insightful discussion. We also acknowledge the support of the MPI-PKS visitors program. G.H.-H.Chuang also thanks EPSRC Grant No. EP/P021123/1 for the provided support.

**Supplementary information.**

## A Derivation of Equation (6) and (7)

First, the explicit form of Lagrangian is derived under the coupled-coherent state representation, and then the Euler-Lagrangian equation is shown for deriving the equation-of-motion of both amplitude and coherent state.

By definition, the Lagrangian is

$$\mathcal{L} = \langle \Psi | i \frac{\hat{\partial}}{\partial t} | \Psi \rangle - \langle \Psi | \hat{H} | \Psi \rangle. \quad (\text{A.1})$$

The first term of equation (A.1) is formed by substituting equation (??) and (4) in it,

$$\langle \Psi | i \frac{\hat{\partial}}{\partial t} | \Psi \rangle = i \sum_{m,l}^N \bar{a}_m \dot{a}_l \langle \xi_m | \xi_l \rangle + \bar{a}_m a_l \langle \xi_m | \dot{\xi}_l \rangle, \quad (\text{A.2})$$

where the first term has an overlap matrix element,  $\langle \xi_m | \xi_l \rangle = \Omega_{ml}$  and its explicit form is shown in equation (5). In the second term,  $\langle \xi_m | \dot{\xi}_l \rangle$  is

$$\begin{aligned} \langle \xi_m | \dot{\xi}_l \rangle &= \left( \bigotimes_i^M \langle \xi_m^i | \right) \left( \sum_{j \neq k}^M \langle \dot{\xi}_l^j | \bigotimes_k^{M-1} | \xi_l^k \rangle \right) \\ &= \left( \bigotimes_i^M \langle \xi_m^i | \right) \left( \sum_{j \neq k}^M \frac{d}{dt} \left[ \frac{(\xi_l^j + 1) |0\rangle + (\xi_l^j - 1) |1\rangle}{\sqrt{2(1 + \bar{\xi}_l^j \xi_l^j)}} \right] \bigotimes_k^{M-1} | \xi_l^k \rangle \right) \\ &= \left( \sum_i^M \frac{\bar{\xi}_m^i \dot{\xi}_l^i}{1 + \bar{\xi}_m^i \xi_l^i} - \frac{\dot{\xi}_l^i \xi_m^i + \bar{\xi}_l^i \dot{\xi}_l^i}{2(1 + \bar{\xi}_l^i \xi_l^i)} \right) \left( \prod_i^M \frac{1 + \bar{\xi}_m^i \xi_l^i}{\sqrt{1 + \bar{\xi}_m^i \xi_m^i} \sqrt{1 + \bar{\xi}_l^i \xi_l^i}} \right) \\ &:= (M_{ml})(\Omega_{ml}) \\ &:= \chi_{ml} \end{aligned}$$

The second term of equation (A.1) has a term that depends on the Hamiltonian

$$\begin{aligned} -\langle \Psi | \hat{H} | \Psi \rangle &= - \sum_{m,l}^N \bar{a}_m a_l \langle \xi_m | \hat{H} | \xi_l \rangle \\ &= - \sum_{m,l}^N \bar{a}_m a_l H_{ml}. \end{aligned}$$

Plug equation (A.3) in equation (A.2), and then combine equation (A.3), the explicit form of Lagrangian becomes

$$\mathcal{L} = \sum_{m,l}^N i\bar{a}_m \dot{a}_l \Omega_{ml} + i\bar{a}_m a_l \chi_{ml} - \bar{a}_m a_l H_{ml}. \quad (\text{A.3})$$

The only unknown term for now is  $H_{ml}$ , which is depends on the explicit form of Hamiltonian.

From the Euler-Lagrange equations, the equation-of-motion of amplitude ( $a(t)$ ) is

$$\frac{d}{dt} \left( \frac{\partial \mathcal{L}}{\partial \dot{a}_m} \right) - \frac{\partial \mathcal{L}}{\partial a_m} = 0. \quad (\text{A.4})$$

Since the equation (A.3) is not a function of  $\dot{a}_m$ , the first term of the above equation is zero. And the second term is  $\frac{\partial \mathcal{L}}{\partial a_m} = 0$ , which resulting the equation-of-motion of amplitude is

$$\frac{\partial \mathcal{L}}{\partial a_m} = \sum_{m,l}^N i \Omega_{ml} \dot{a}_l + i \chi_{ml} a_l - H_{ml} a_l = 0. \quad (\text{A.5})$$

Rewrite the above equation into matrix form, which is

$$\dot{\mathbf{a}} = \boldsymbol{\Omega}^{-1} (-\boldsymbol{\chi} - i \mathbf{H}) \mathbf{a}. \quad (\text{A.6})$$

The equation of motion of coherent state is

$$\dot{\xi}_l^i = -i \frac{\partial \langle \boldsymbol{\xi}_l | \hat{H} | \boldsymbol{\xi}_l \rangle}{\partial \bar{\xi}_l^i} (1 + \bar{\xi}_l^i \xi_l^i)^2. \quad (\text{A.7})$$

From equations (A.6) and (A.7), the only unknown terms are  $H_{ml}$  and  $\frac{\partial \langle \boldsymbol{\xi}_l | \hat{H} | \boldsymbol{\xi}_l \rangle}{\partial \bar{\xi}_l^i}$ .

From Ref [20], the time-dependent Hamiltonian is given in equation (3). All the interactions between neighbours are considered. After plugin the equation (4),  $H_{ml}$  is

$$\begin{aligned} H_{ml} = \langle \boldsymbol{\xi}_m | \hat{H} | \boldsymbol{\xi}_l \rangle &= \left( \frac{\Omega(t)}{2} \sum_i^M \frac{\bar{\xi}_m^i \xi_m^i - 1}{1 + \bar{\xi}_m^i \xi_l^i} - \frac{\Delta(t)}{2} \sum_i^M \frac{(\bar{\xi}_m^i - 1)(\xi_l^i - 1)}{1 + \bar{\xi}_m^i \xi_l^i} \right. \\ &\quad \left. + \sum_{i \neq j}^M \frac{V_{ij}}{4} \frac{(\bar{\xi}_m^i - 1)(\xi_l^i - 1)}{1 + \bar{\xi}_m^i \xi_l^i} \frac{(\bar{\xi}_m^j - 1)(\xi_l^j - 1)}{1 + \bar{\xi}_m^j \xi_l^j} \right) \Omega_{ml}. \end{aligned} \quad (\text{A.8})$$

Replace dummy index  $m$  to  $l$  and then take derivative with respective to  $\bar{\xi}_l^i$ ,

$$\frac{\partial \langle \xi_l | \hat{H} | \xi_l \rangle}{\partial \bar{\xi}_l^i} = \frac{1}{(1 + \bar{\xi}_l^i \xi_l^i)^2} \left( \Omega(t) \xi_l^i + \frac{(\xi_l^i)^2 - 1}{2} \left( -\Delta(t) + \sum_{i \neq j}^M V_{ij} \frac{(\bar{\xi}_l^j - 1)(\xi_l^j - 1)}{1 + \bar{\xi}_l^j \xi_l^j} \right) \right). \quad (\text{A.9})$$

Finally, the explicit form of the equations of motion for both amplitudes  $a_l(t)$  and coherent states  $|\xi_l(t)\rangle$  are

$$\begin{aligned} \dot{\mathbf{a}} &= \boldsymbol{\Omega}^{-1}(-\boldsymbol{\chi} - i \mathbf{H}) \mathbf{a}, \\ \dot{\xi}_l^i &= -i \left( \Omega(t) \xi_l^i + \frac{(\xi_l^i)^2 - 1}{2} \left( -\Delta(t) + \sum_{j \neq i}^M V_{ij} \frac{(\bar{\xi}_l^j - 1)(\xi_l^j - 1)}{\bar{\xi}_l^j \xi_l^j + 1} \right) \right). \end{aligned} \quad (\text{A.10})$$

Equation (A.10) is written in the vector-matrix form, and the explicit form of three matrices, and  $\boldsymbol{\Omega}$ ,  $\boldsymbol{\chi}$ , and  $\mathbf{H}$ , are shown in equation (5), (A.3) and (A.8), respectively.

## B Derivation of Equation (8)

We list all the possible micro-configuration under specific limitation to derive the sum of configuration. For example, the total configuration of qubit chain is  $2^N$  where  $N$  is number of qubit. To consider the micro-configuration, let the number of Rydberg state is  $y$ , and the number of ground state be  $N - y$ . If there is no Rydberg state in a chain, there is only one configuration  $|gggg \dots\rangle$ , where all qubits are in ground state. If there is one and only one Rydberg state in a chain, the number of micro-configuration is  $N$ . List all the possible conditions as following equation,

$$C_{\text{tot}} = \binom{N}{0} + \binom{N}{1} + \dots + \binom{N}{y} + \dots + \binom{N}{N} = \sum_{y=0}^N \frac{N!}{(N-y)!y!} = 2^N \quad (\text{B.11})$$

Now, we consider a chain with isolate Rydberg state. Let the number  $M$  be the number of dimer configuration ( $|rg\rangle$  or  $|gr\rangle$ ), and it depends on the total number of the chain  $N$ . The maximum number of this dimer is  $M = N//2 + 1$ , where  $N//2$  is the quotient of  $N$  divides by 2. If the number of ground state ( $N - y$ ) is equal to the number of Rydberg state ( $y$ ), then  $M = N/2 = N//2$ . The condition of  $M$  is then

$$M = \begin{cases} N//2 & \text{for } N - y = y \\ N//2 + 1 & \text{for } N - y \neq y, \end{cases} \quad (\text{B.12})$$

The vacancy between ground state is  $N - y + 1$  for considering the two ends in a chain. Place the above dimer into possible vacancy, and then the resulting configuration of isolated Rydberg state in a chain is

$$C_{\text{iso}} = \binom{N - y + 1}{0} + \binom{N - y + 1}{1} + \dots + \binom{N - y + 1}{y} + \dots + \binom{N - y + 1}{M}$$

$$= \sum_{y=0}^M \frac{(N-y+1)!}{(N-2y+1)!y!} \quad (\text{B.13})$$

Finally, we consider only one pair of Rydberg state  $|rr\rangle$  in a chain. Without this pair of Rydberg state, the rest number of chain is  $N-2$  and the maximum number of the Rydberg state in this remaining chain is  $\frac{N-2}{2}$ . So the maximum number of Rydberg state in a chain is  $O = \frac{N-2}{2} + 2$ . We place this pair of Rydberg state in a chain first, and its possible configuration is  $N-y+1$ . Secondly, we place the remaining Rydberg state in the rest vacancy  $N-y$ . The total configuration is

$$\begin{aligned} C_{\text{pair}} &= (N-y+1) \times \left( \binom{N-y}{0} + \binom{N-y}{1} + \cdots + \binom{N-y}{y-2} + \cdots + \binom{N-y}{O} \right) \\ &= \sum_{y=2}^O \frac{(N-y+1)!}{(N-2y+2)!(y-2)!} \end{aligned} \quad (\text{B.14})$$

## References

- [1] V. Lienhard, S. de Léséleuc, D. Barredo, T. Lahaye, A. Browaeys, M. Schuler, L.P. Henry, A.M. Läuchli, Observing the space-and time-dependent growth of correlations in dynamically tuned synthetic ising models with antiferromagnetic interactions. *Physical Review X* **8**(2), 021070 (2018)
- [2] A. Browaeys, T. Lahaye, Many-body physics with individually controlled rydberg atoms. *Nature Physics* **16**(2), 132–142 (2020)
- [3] P. Schauss, Quantum simulation of transverse ising models with rydberg atoms. *Quantum Science and Technology* **3**(2), 023001 (2018)
- [4] H. Bernien, S. Schwartz, A. Keesling, H. Levine, A. Omran, H. Pichler, S. Choi, A.S. Zibrov, M. Endres, M. Greiner, et al., Probing many-body dynamics on a 51-atom quantum simulator. *Nature* **551**(7682), 579–584 (2017)
- [5] A. Keesling, A. Omran, H. Levine, H. Bernien, H. Pichler, S. Choi, R. Samajdar, S. Schwartz, P. Silvi, S. Sachdev, et al., Quantum kibble–zurek mechanism and critical dynamics on a programmable rydberg simulator. *Nature* **568**(7751), 207–211 (2019)
- [6] D.S. Ding, Z.K. Liu, B.S. Shi, G.C. Guo, K. Mølmer, C.S. Adams, Enhanced metrology at the critical point of a many-body rydberg atomic system. *Nature Physics* **18**(12), 1447–1452 (2022)
- [7] C.S. Adams, J.D. Pritchard, J.P. Shaffer, Rydberg atom quantum technologies. *Journal of Physics B: Atomic, Molecular and Optical Physics* **53**(1), 012002 (2019)
- [8] D. Barredo, H. Labuhn, S. Ravets, T. Lahaye, A. Browaeys, C.S. Adams, Coherent excitation transfer in a spin chain of three rydberg atoms. *Physical review letters* **114**(11), 113002 (2015)
- [9] J. Wilson, S. Saskin, Y. Meng, S. Ma, R. Dilip, A. Burgers, J. Thompson, Trapping alkaline earth rydberg atoms optical tweezer arrays. *Physical review letters* **128**(3), 033201 (2022)

- [10] M. Moreno-Cardoner, D. Goncalves, D.E. Chang, Quantum nonlinear optics based on two-dimensional rydberg atom arrays. *Physical Review Letters* **127**(26), 263602 (2021)
- [11] J.J. Sakurai, *Modern Quantum Mechanics, Revised Edition*, rev. ed. edn. (Pearson, Upper Saddle River, NJ, 1993)
- [12] W. Schweizer, *Numerical Quantum Dynamics, Progress in theoretical chemistry and physics*, vol. 9 (Springer Science & Business Media, Dordrecht, 2006)
- [13] A. Persson, Numerical methods for solving the time-dependent Schrödinger equation. *Student Paper* (2012)
- [14] R.G. Littlejohn, M. Cargo, T. Carrington, K.A. Mitchell, B. Poirier, A general framework for discrete variable representation basis sets **116**(20), 8691–8703 (2002)
- [15] S.P. Webb, S. Hammes-Schiffer, Fourier grid hamiltonian multiconfigurational self-consistent-field: A method to calculate multidimensional hydrogen vibrational wavefunctions. *J. Chem. Phys.* **113**(13), 5214–5227 (2000)
- [16] J.C. Light, T. Carrington, Jr., Discrete-variable representations and their utilization pp. 263–310 (2007)
- [17] D.T. Colbert, W.H. Miller, A novel discrete variable representation for quantum mechanical reactive scattering via the s-matrix kohn method. *J. Chem. Phys.* **96**(3), 1982–1991 (1992)
- [18] J.H. Baraban, A.R. Beck, A.H. Steeves, J.F. Stanton, R.W. Field, Reduced dimension discrete variable representation study of cis-trans isomerization in the S1 state of C2H2. *J. Chem. Phys.* **134**(24), 244311 (2011)
- [19] E. Titov, A. Humeniuk, R. Mitric, Comparison of moving and fixed basis sets for nonadiabatic quantum dynamics at conical intersections. *Chem. Phys.* **528**, 110526 (2020)
- [20] H. Bernien, S. Schwartz, A. Keesling, H. Levine, A. Omran, H. Pichler, S. Choi, A.S. Zibrov, M. Endres, M. Greiner, V. Vuletić, M.D. Lukin, Probing many-body dynamics on a 51-atom quantum simulator. *Nature* **551**(7682), 579–584 (2017)
- [21] C.J. Turner, A.A. Michailidis, D.A. Abanin, M. Serbyn, Z. Papić, Quantum scarred eigenstates in a Rydberg atom chain: Entanglement, breakdown of thermalization, and stability to perturbations. *Phys. Rev. B Condens. Matter* **98**(15), 155134 (2018)
- [22] J. Johansson, P. Nation, F. Nori, QuTiP: An open-source Python framework for the dynamics of open quantum systems. *Computer Physics Communications* **183**(8), 1760–1772 (2012)
- [23] J. Johansson, P. Nation, F. Nori, QuTiP 2: A Python framework for the dynamics of open quantum systems. *Computer Physics Communications* **184**(4), 1234–1240 (2013)